Monthly Notices
of the
ROYAL ASTRONOMICAL SOCIETY

MNRAS **481,** L21–L25 (2018)
Advance Access publication 2018 August 13

doi:10.1093/mnrasl/sly148

The Galactic warp revealed by *Gaia* DR2 kinematics

E. Poggio,[1,2★] R. Drimmel,[2] M. G. Lattanzi,[2] R. L. Smart,[2] A. Spagna,[2] R. Andrae,[3] C. A. L. Bailer-Jones,[3] M. Fouesneau,[3] T. Antoja,[4] C. Babusiaux,[5,6] D. W. Evans,[7] F. Figueras,[4] D. Katz,[7] C. Reylé,[8] A. C. Robin,[8] M. Romero-Gómez[4] and G. M. Seabroke[9]

[1] *Università di Torino, Dipartimento di Fisica, via P. Giuria 1, I-10125, Torino, Italy*
[2] *Osservatorio Astrofisico di Torino, Istituto Nazionale di Astrofisica (INAF), I-10025 Pino Torinese, Italy*
[3] *Max Planck Institute for Astronomy, Königstuhl 17, D-69117 Heidelberg, Germany*
[4] *Institut de Ciències del Cosmos, Universitat de Barcelona (IEEC-UB), Martí i Franquès 1, E-08028 Barcelona, Spain*
[5] *Univ. Grenoble Alpes, CNRS, IPAG, F-38000 Grenoble, France*
[6] *GEPI, Observatoire de Paris, Université PSL, CNRS, 5 Place Jules Janssen, F-92190 Meudon, France*
[7] *France Institute of Astronomy, University of Cambridge, Madingley Road, Cambridge CB3 0HA, UK*
[8] *Institut UTINAM, CNRS UMR6213, Univ. Bourgogne Franche-Comté, OSU THETA Franche-Comté-Bourgogne, Observatoire de Besançon, BP 1615, F-25010 Besançon Cedex, France*
[9] *Mullard Space Science Laboratory, University College London, Holmbury St Mary, Dorking, Surrey RH5 6NT, United Kingdom*

Accepted 2018 August 8. Received 2018 July 27; in original form 2018 May 8

ABSTRACT

Using *Gaia* DR2 astrometry, we map the kinematic signature of the Galactic stellar warp out to a distance of 7 kpc from the Sun. Combining *Gaia* DR2 and 2-Micron All Sky Survey photometry, we identify, via a probabilistic approach, 599 494 upper main sequence (UMS) stars and 12 616 068 giants without the need for individual extinction estimates. The spatial distribution of the UMS stars clearly shows segments of the nearest spiral arms. The large-scale kinematics of both the UMS and giant populations show a clear signature of the warp of the Milky Way, apparent as a gradient of 5–6 km s^{-1} in the vertical velocities from 8 to 14 kpc in Galactic radius. The presence of the signal in both samples, which have different typical ages, suggests that the warp is a gravitationally induced phenomenon.

Key words: stars: kinematics and dynamics – Galaxy: disc – Galaxy: kinematics and dynamics – Galaxy: structure.

1 INTRODUCTION

The disc of our Galaxy was first seen to be warped in the radio observations of neutral hydrogen more than 60 years ago (Kerr 1957). Later observations (Freudenreich et al. 1994; Drimmel & Spergel 2001; López-Corredoira et al. 2002b; Robin, Reylé & Marshall 2008; Reylé et al. 2009; Amôres, Robin & Reylé 2017, and others) also showed that the stellar disc is flat out to roughly the Solar Circle, then bends up upwards in the north and downwards in the south, with the Sun close to the line of nodes. Theoretical models for the warping of stellar discs include interactions with satellites (Kim et al. 2014), intergalactic magnetic fields (Battaner 1990), accretion of intergalactic matter (Kahn & Woltjer 1959; López-Corredoira, Betancort-Rijo & Beckman 2002a), and a misaligned dark halo (Sparke & Casertano 1988; Debattista & Sellwood 1999), amongst others. However, to date only the shape of the Galactic warp has been roughly constrained, leading to a lack of consensus for its causal mechanism due to the lack of kinematic information perpendicular to the Galactic disc. In particular, a consistent kinematic signature in old and young stars would exclude non-gravitational mechanisms (see Section 4). In the pre-*Gaia* era, kinematic studies suggested a signature inconsistent with a long-lived warp (Smart et al. 1998; Drimmel, Smart & Lattanzi 2000; López-Corredoira et al. 2014), while the kinematics of stars near the Sun seemed to be consistent with the presence of a warp (Dehnen 1998, though see Seabroke & Gilmore 2007). With the first *Gaia* data release, Schönrich & Dehnen (2018) detected the warp kinematic signature using the TGAS catalogue, while Poggio et al. (2017) found no evidence of the warp signal in the kinematics of OB stars.

With *Gaia*'s most recent second data release, Gaia Collaboration (2018) (hereafter MWDR2) showed a kinematic signature on large scales consistent with a warp with a sample of red giants (in agreement with LAMOST radial velocities, Liu, Tian & Wan 2017), while their young OB stellar sample seemed to give divergent results. In this contribution we expand on the work of MWDR2, with larger and fainter samples of the old (red giants) and young (upper

---

★ E-mail: eloisa.poggio@inaf.it

Published by Oxford University Press on behalf of the Royal Astronomical Society

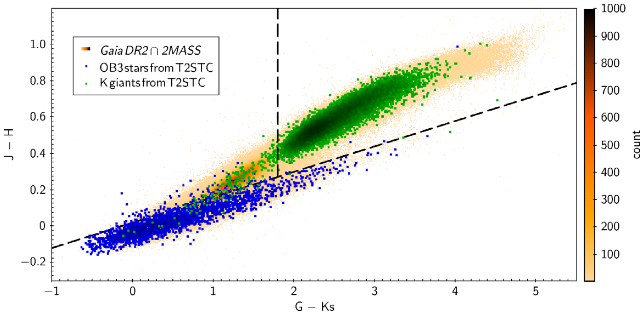

Figure 1. Colour–colour plot showing the 2MASS-*Gaia*preliminary selection. Candidate UMS are taken as stars lying below the diagonal dashed line, while candidate giants are those lying in the top right area of the plots. A similar plot (here not shown) was constructed with $(J - K_s)$ on the vertical axis. The yellow–orange density plots a sample of *Gaia* DR2 stars with $G < 12$, while the blue and green points show the colours of stars in the T2STC that are classified as either OB stars or K giants (luminosity class I and II).

main sequence stars) selected from *Gaia* DR2, using 2-Micron All Sky Survey (2MASS, Skrutskie et al. 2006) photometry (Section 2). We compare the kinematic maps of these two samples (Section 3) and discuss the obtained results (Section 4).

2 DATA SELECTION

To select upper main sequence (UMS) and giants in the Galactic plane ($|b| < 20$ deg) without the need for individual reddening estimates, we use 2MASS photometry for *Gaia* DR2 sources using the cross match table provided by the *Gaia* Archive (`https://archives.esac.esa.int/gaia`), and restricting ourselves to 2MASS sources with uncertainties $\sigma_{J,H,K_s} < 0.05$ mag and a photometric quality flag of 'AAA'. Finally, as a practical matter, we select stars with $G < 15.5$ mag, as very few fainter stars have 2MASS photometry.

UMS stars. A preliminary selection is made based only on measured 2MASS/*Gaia* colours. As shown in Fig. 1, known OB stars from the Tycho-2 Spectral Type Catalogue (hereafter T2STC, Wright et al. 2003) lie along a sequence that is a consequence of interstellar reddening, which is clearly separated from the redder turn-off stars, giants, and lower main sequence stars. Based on this, candidates UMS stars are selected from the Gaia DR2∩2MASS catalogue satisfying both $(J - H) < 0.14\,(G - K_s) + 0.02$ and $(J - K) < 0.23\,(G - K_s)$.

A second step of the selection procedure uses *Gaia* astrometry (Lindegren et al. 2018), choosing those stars whose parallax ϖ, parallax uncertainty σ_ϖ, and apparent G magnitude is likely to be consistent with being a UMS star. To this end, we calculated the probability density function (PDF) of the heliocentric distance r for the given coordinates (l, b) via Bayes' theorem, $P(r\,|l, b, \varpi, \sigma_\varpi) \propto P(\varpi\,|r, \sigma_\varpi)\,P(r|l, b)$, assuming a Gaussian likelihood $P(\varpi\,|r, \sigma_\varpi)$ and constructing the prior according to Astraatmadja & Bailer-Jones (2016) (their equation 7, i.e. the Milky Way prior)

$$P(r|l, b) \propto r^2\,\rho(l, b, r)\,S(l, b, r). \tag{1}$$

We adopt a simple density model for the Galactic disc $\rho(l, b, r)$, consisting of an exponential disc in Galactocentric radius R and vertical height z, with a radial scale length $L_R = 2.6$ kpc (Bland-Hawthorn & Gerhard 2016) and vertical scale height $h_z = 150$ pc (larger than the known scale height for OB stars, Poggio et al. 2017). We assume for the Sun $R_\odot = 8.34$ kpc (Reid et al. 2014) and $z_\odot = 25$ pc (Bland-Hawthorn & Gerhard 2016). The term $S(l, b, r)$ takes into account the fall-off of the number of observable objects with r due to the survey selection function, neglect of which can cause severe biases in the obtained distance estimates (Schönrich & Aumer 2017). We estimated the term $S(l, b, r)$ according to Astraatmadja & Bailer-Jones (2016), and modelled the variation of Gaia DR2∩2MASS completeness as a function of apparent magnitude G according to Drimmel et al. (in prep.), including the previously mentioned cut at $G = 15.5$. The adopted luminosity function in the G band is calculated through the PARSEC isochrones (web interface `http://stev.oapd.inaf.it/cmd`, Bressan et al. 2012; Chen et al. 2014, 2015; Tang et al. 2014), after taking into account the colour–colour cuts applied in the preliminary selection. The luminosity function was obtained assuming a star formation rate constant with time, the canonical two-part power law IMF corrected for unresolved binaries (Kroupa 2001, 2002), and solar metallicity. The impact of various assumptions incorporated in our prior is discussed in the following section.

For each star, we derived from $P(r\,|l, b, \varpi, \sigma_\varpi)$ a PDF of the quantity $M' \equiv M_G + A_G = G - 5\log r_{\rm pc} + 5$, which is the absolute magnitude M_G plus the extinction in the G band of the source. The Jacobian of the transformation $\mathrm{d}r/\mathrm{d}M'$ can be written when the G magnitude is fixed, obtaining $P(M'|l, b, \varpi, \sigma_\varpi, G)$. After numerically imposing the normalization condition $\int_{-\infty}^{+\infty} P(M'|l, b, \varpi, \sigma_\varpi, G)dM' = 1$, we calculate the probability of the star being brighter than the limit M'_{lim}, which is the faintest extincted magnitude that we are willing to tolerate for a UMS star candidate with an observed $(G - K_s)$ colour. The tolerance limit M'_{lim} was arbitrarily chosen as the absolute magnitude of a fictitious B3-like star having $\log\,(\mathrm{age/yr}) = 6$ and $\log\,(T_{\rm eff}) = 4.27$. For such a star, the PARSEC isochrones provide us with an absolute magnitude of $(M_G)_{\rm lim} = -0.7$ and $(G - K_s) = -0.6$ in the case of no extinction. The PARSEC isochrones give the corresponding values of M'_{lim} and $(G - K_s)$ when extinction is present (Fig. 2, left plot).

Hence we calculate the probability of the star being a UMS star – i.e. brighter than the tolerance limit – by performing the following integral

$$p(UMS\,|\,l, b, \varpi, \sigma_\varpi, G) = \int_{-\infty}^{M'_{lim}} P(M'|l, b, \varpi, \sigma_\varpi, G)\,dM', \tag{2}$$

which is by definition between 0 and 1. The stars for which $p(UMS\,|\,l, b, \varpi, \sigma_\varpi, G) > 0.5$ are selected, giving us 599 494 UMS stars.

Giant stars. In a similar fashion as the colour–colour selection of the UMS stars, we perform a preliminary selection based on photometry, this time selecting the stars with $(J - H) > 0.14\,(G - Ks) + 0.02$ and $(J - Ks) > 0.23\,(G - Ks)$ (see Fig. 1), with an additional $(G - Ks) > 1.8$ cut to remove the objects too blue to be considered giant candidates. We adopt the same probabilistic approach used for the UMS stars, but assuming a spatial density scale height of $h_z = 300$ pc (Bland-Hawthorn & Gerhard 2016). We calculate for each source the probability of being a giant star, with the tolerance limit set as equal to $M'_{lim} = 1.3\,(G - Ks) - 1.7$. Such a limit removes subgiants and dwarfs, and also accounts for interstellar reddening (see Fig. 2, right plot). This selection gives us 12 616 068 giants.

To test the composition of the selected samples, we crossmatched our samples with the T2STC. For the UMS sample, we obtained 24 422 objects, of which approximately 55 per cent are OB stars, 40 per cent are A stars, and 5 per cent are F stars, according to the T2STC spectral classifications. For the giant sample, we found

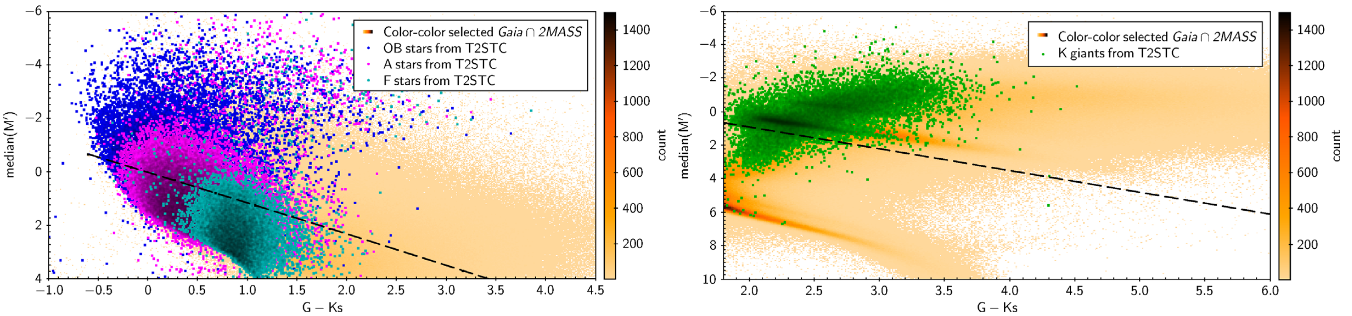

Figure 2. The parallax criterion for the UMS (left-hand panel) and for the giants (right-hand panel). On the *y*-axis, the median of the PDF of $M^{'}$. The dashed line shows the adopted tolerance limit (see text), selecting those stars that are above the dashed lines. Orange density area as in the previous plot, other coloured points are for those stars in the T2STC, colour coded as per the key in the figures.

33 842 stars with complete spectral classification from T2STC, of which 88 per cent are giants (69 per cent K giants and 19 per cent G giants) and 12 per cent are main sequence stars (mostly of spectral class K or G, while A or F stars are less than 1 per cent).

3 DENSITY AND KINEMATIC MAPS

In this section, we present and compare the maps obtained with the UMS and giant samples, shown in Fig. 3. For both samples we use as our distance estimator for each star the mean (see for example Gelman et al. 1995; MacKay 2003) of the posterior distribution $P(r\,|l, b, \varpi, \sigma_{\varpi})$ (see previous section). The UMS stars have mean distances of approximately 3 kpc, and mean heights with respect to the Galactic plane of about 100 pc, in contrast to the giant sample, which presents, respectively, 4.5 kpc and 480 pc. The giant sample exhibits a smooth density distribution (Fig. 3B), decreasing for large heliocentric distance, as expected for a magnitude limited sample, and for larger Galactocentric radii, as expected from an exponential disc. In contrast the UMS sample (Fig. 3A) shows three observed overdensities that correspond to sections of the nearby spiral arms (from left to right: Sagittarius–Carina arm, local arm, and Perseus arm). The evident spiral structure confirms that our UMS sample is young with respect to the smooth distribution shown by the older and dynamically relaxed giant population.

Figs 3c and d show a face-on view of the vertical motions in the Galactic plane of the two samples, calculated deriving the proper motions in galactic latitude $\mu_{\rm b}$ from the *Gaia* DR2 astrometry and correcting for the solar motion $(V_{X\odot}, V_{Y\odot}, V_{Z\odot}) = (11.1, 12.24, 7.25)$ km s^{-1} (Schönrich, Binney & Dehnen 2010). The large majority of stars in our UMS sample lack line-of-sight velocities, so that it is not possible to calculate directly the vertical velocity. We therefore estimate the mean vertical velocity V_Z' from the available astrometry, correcting for solar motion and differential Galactic rotation, assuming a flat rotation curve ($V_{\rm c} = 240$ km s^{-1}, Reid et al. 2014), as done in MWDR2 (see equation 8 of Drimmel et al. 2000). We find that 3 042 265 of our giants have line-of-sight velocities provided in *Gaia* DR2, for which we calculate directly the vertical velocity, while for the remaining we estimate the vertical velocities as done for the UMS sample. (For the subsample of star having line-of-sight velocities, we have verified that our approximation of using V_Z' instead of V_Z produces consistent results.)

A gradient in the median vertical velocities is apparent in Figs 3c and d, as expected from a warp signature (Abedi et al. 2014; Poggio et al. 2017). Also worthy to note is that the peak velocities in both samples is not exactly towards the anticentre, which is probably due to the Sun not being on the line of nodes. Radial features in this plot are due to uneven sampling above/below the Galactic plane due to foreground extinction (see Section 8.4.2 in the Gaia DR2 online documentation). The bootstrap uncertainties on the median velocities $\sigma^*_{V_Z}$ are shown in Figs 3e and f. The systematic increase of the median vertical velocity is of about 5–6 km s^{-1} from $R \sim 8$ kpc to 14 kpc, with a signal-to-noise greater than 10. The subsets of stars having $\varpi/\sigma_{\varpi} > 5$ (478 258 UMS stars and 6 373 188 giants) present a signal consistent with the whole sample. In order to test the robustness of the signal, we also recalculated distances with the iterative approach of Schönrich & Aumer (2017) for $20^o < l < 340^o$, finding a consistent gradient. We also slightly modified the prior (e.g. assuming $L_R = 4$ kpc for the UMS sample or including a thick disc for the giant sample), always confirming the presence of the signal. Moreover, we verified that adopting as distance estimator the mode (following Bailer-Jones 2015; Bailer-Jones 2017; Bailer-Jones et al. 2018) or the median of the PDF produces consistent results. Finally, we explored the impact of a systematic zero-point error (exploring the range ±0.080 mas) of *Gaia* DR2 parallaxes (Lindegren et al. 2018), which only results in a contraction/expansion of the maps, but still preserves the presence of the warp signature.

4 DISCUSSION AND CONCLUSIONS

The kinematic signature of the Galactic warp is expected to manifest itself towards the Galactic anticentre as large-scale systematic velocities perpendicular to the Galactic plane. Thanks to the large sample of stars in *Gaia* DR2 with exquisite astrometric precision, we are able to map the vertical motions over a larger extent of the Milky Way's disc than previously possible, for both an intrinsically young and old population. That our UMS sample clearly shows the spiral arms, in contrast with the giant population, confirms that it is a dynamically young population.

The observed gradient in the giants appears to be in agreement with the overall increase in vertical velocity shown by *Gaia* DR2 data in Kawata et al. (2018) and the giant sample in MWDR2 for the range in Galactocentric radius in which our studies overlap. Meanwhile, our UMS sample exhibit a more perturbed pattern than the giants at $R < 12$ kpc, in agreement with the OB sample in MWDR2, showing the warp signature at larger Galactocentric radii.

The presence of the warp signature in our two samples suggests that the warp is principally a gravitational phenomenon; indeed, warp generation models exclusively based on non-gravitational mechanisms (such as magnetic fields or hydrodynamical pressure from infalling gas) would act on the gas and affect the young stars only (see also the discussion in Guijarro et al. 2010; Sellwood

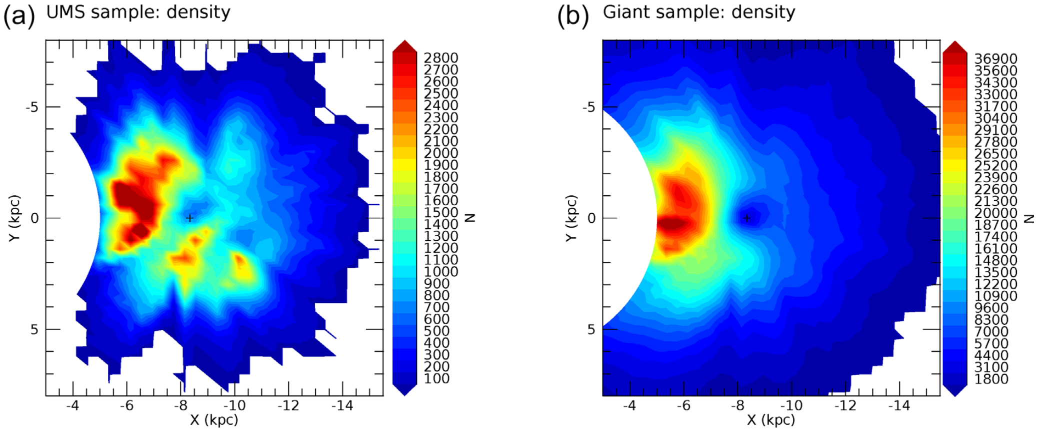

(a) UMS sample: density

(b) Giant sample: density

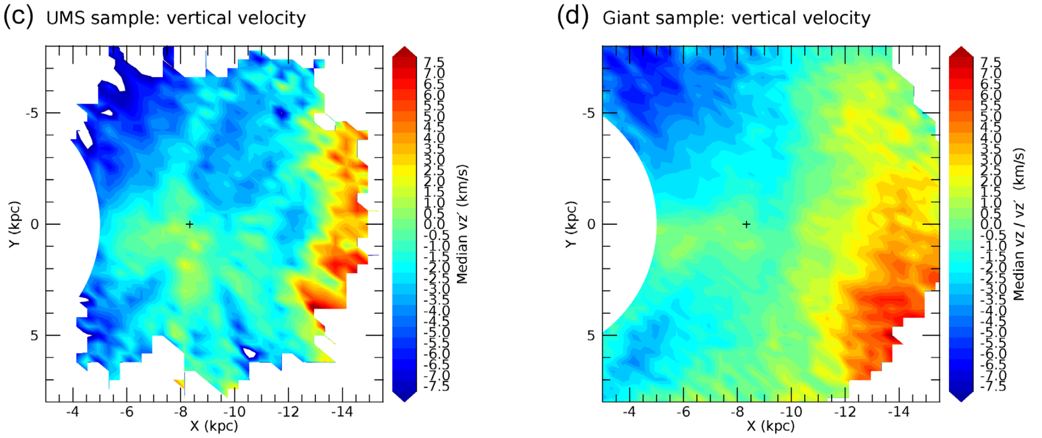

(c) UMS sample: vertical velocity

(d) Giant sample: vertical velocity

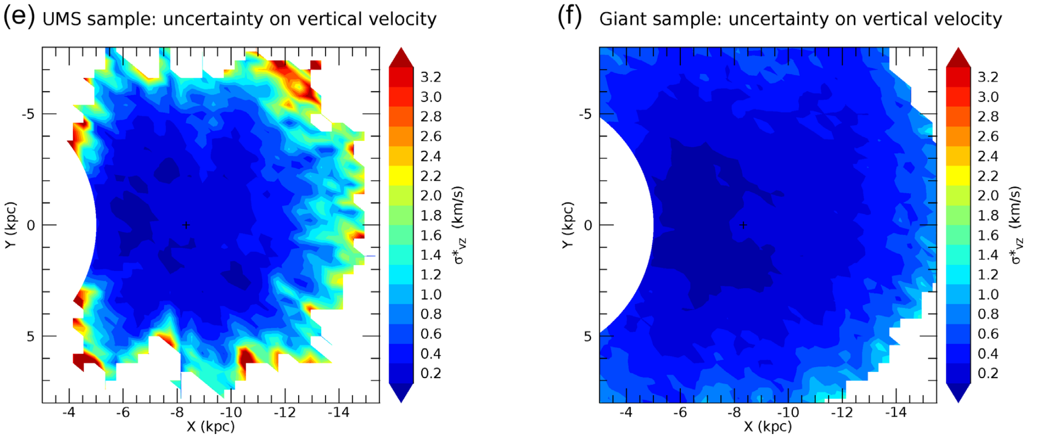

(e) UMS sample: uncertainty on vertical velocity

(f) Giant sample: uncertainty on vertical velocity

Figure 3. Maps for the UMS (left plots) and giant (right plots) samples. The Sun is represented by a black cross at X = −8.35 kpc and Y = 0 kpc. The Galactic centre is located at X = 0 and Y = 0, and the Galaxy is rotating clockwise. The XY plane was divided into cells of 400 pc width, only showing the ones containing more than 50/500 stars for the UMS/giant sample. From top to bottom: maps of the density (N is the number of sources per cell), median vertical velocity V_Z or V'_Z (see text), and bootstrap uncertainty on the median vertical velocity $\sigma^*_{V_Z}$.

2013); recently-born stars would inherit the kinematics of the gas and trace the warp-induced kinematics until phase mixing smeared out evidence of their initial conditions. The detection of a similar warp kinematic signal in both young and old stellar populations thus suggests that gravity is the principle mechanism causing the warp. However, the two samples do present some differences on smaller scales, possibly indicating that additional perturbations or forces are acting on the gaseous component of the disc.

Here, we have only evidenced the kinematic signature of the warp in *Gaia* DR2. Our findings bear further witness to the great potential of this data set. Future work confronting this signature with more quantitative models will certainly reveal further details of the dynamical nature of the Galactic warp.

ACKNOWLEDGEMENTS

This work uses data products from: the ESA *Gaia* mission (gea.esac.esa.int/archive/), funded by national institutions participating in the *Gaia* Multilateral Agreement; and the Two Micron All Sky Survey (2MASS, www.ipac.caltech.edu/2mass). This work was supported by ASI (Italian Space Agency) under contract 2014-025-R.1.2015 and the MINECO (Spanish Ministry of Economy) through grant ESP2016-80079-C2-1-R (MINECO/FEDER, UE) and MDM-2014-0369 of ICCUB (Unidad de Excelencia 'Mara de Maeztu'). EP acknowledges the financial support of the 2014 PhD fellowship programme of the INAF (Istituto Nazionale di Astrofisica). This project was developed in part at the 2016 NYC Gaia Sprint, hosted by the Center for Computational Astrophysics at the Simons Foundation in New York City.

REFERENCES

Abedi H., Mateu C., Aguilar L. A., Figueras F., Romero-Gómez M., 2014, MNRAS, 442, 3627

Amôres E. B., Robin A. C., Reylé C., 2017, A&A, 602, A67

Astraatmadja T. L., Bailer-Jones C. A. L., 2016, ApJ, 832, 137

Bailer-Jones C. A. L., 2015, PASP, 127, 994

Bailer-Jones C. A. L., 2017, Practical Bayesian Inference: A Primer for Physical Scientists. Cambridge University Press, Cambridge

Bailer-Jones C. A. L., Rybizki J., Fouesneau M., Mantelet G., Andrae R., 2018, AJ, 156, 58

Battaner E. e. a., 1990, A&A, 236, 1

Bland-Hawthorn J., Gerhard O., 2016, ARA&A, 54, 529

Bressan A., Marigo P., Girardi L., Salasnich B., Dal Cero C., Rubele S., Nanni A., 2012, MNRAS, 427, 127

Chen Y., Girardi L., Bressan A., Marigo P., Barbieri M., Kong X., 2014, MNRAS, 444, 2525

Chen Y., Bressan A., Girardi L., Marigo P., Kong X., Lanza A., 2015, MNRAS, 452, 1068

Debattista V. P., Sellwood J. A., 1999, ApJ, 513, L107

Dehnen W., 1998, AJ, 115, 2384

Drimmel R., Spergel D. N., 2001, ApJ, 556, 181

Drimmel R., Smart R. L., Lattanzi M. G., 2000, A&A, 354, 67

Freudenreich H. T. et al., 1994, ApJ, 429, L69

Gaia Collaboration, Katz D., et al., 2018, A&A, 616, A11

Gelman A., Gelman A., Robert C., Chopin N., Rousseau J., 1995, Bayesian data analysis. p. 1360, 10.1.1.217.2021

Guijarro A., Peletier R. F., Battaner E., Jiménez-Vicente J., de Grijs R., Florido E., 2010, A&A, 519, A53

Kahn F. D., Woltjer L., 1959, ApJ, 130, 705

Kawata D., Baba J., Ciucă I., Cropper M., Grand R. J. J., Hunt J. A. S., Seabroke G., 2018, MNRAS, 479, L108

Kerr F. J., 1957, AJ, 62, 93

Kim J. H., Peirani S., Kim S., Ann H. B., An S.-H., Yoon S.-J., 2014, ApJ, 789, 90

Kroupa P., 2001, MNRAS, 322, 231

Kroupa P., 2002, Science, 295, 82

Lindegren L. et al., A&A, 2018, 616, A2

Liu C., Tian H.-J., Wan J.-C., ed. 2017, Proc. IAU Symp. Vol. 321. The age-kinematical features in the Milky Way outer disk. Kluwer, Dordrecht, p. 6

López-Corredoira M., Betancort-Rijo J., Beckman J. E., 2002a, A&A, 386, 169

López-Corredoira M., Cabrera-Lavers A., Garzón F., Hammersley P. L., 2002b, A&A, 394, 883

López-Corredoira M., Abedi H., Garzón F., Figueras F., 2014, A&A, 572, A101

MacKay D. J. C., 2003, Information Theory, Inference, and Learning Algorithms. Cambridge University Press, Cambridge

Poggio E., Drimmel R., Smart R. L., Spagna A., Lattanzi M. G., 2017, A&A, 601, A115

Reid M. J. et al., 2014, ApJ, 783, 130

Reylé C., Marshall D. J., Robin A. C., Schultheis M., 2009, A&A, 495, 819

Robin A. C., Reylé C., Marshall D. J., 2008, Astron. Nachr., 329, 1012

Schönrich R., Aumer M., 2017, MNRAS, 472, 3979

Schönrich R., Dehnen W., 2018, MNRAS, 478, 3809

Schönrich R., Binney J., Dehnen W., 2010, MNRAS, 403, 1829

Seabroke G. M., Gilmore G., 2007, MNRAS, 380, 1348

Sellwood J. A., 2013, Dynamics of Disks and Warps. Planets, Stars and Stellar Systems. Vol. 5: Galactic Structure and Stellar Populations. p. 923

Skrutskie M. F. et al., 2006, AJ, 131, 1163

Smart R. L., Drimmel R., Lattanzi M. G., Binney J. J., 1998, Nature, 392, 471

Sparke L. S., Casertano S., 1988, MNRAS, 234, 873

Tang J., Bressan A., Rosenfield P., Slemer A., Marigo P., Girardi L., Bianchi L., 2014, MNRAS, 445, 4287

Wright C. O., Egan M. P., Kraemer K. E., Price S. D., 2003, AJ, 125, 359

This paper has been typeset from a TEX/LATEX file prepared by the author.